

T_{reg} cells limit IFN- γ production to control macrophage accrual and phenotype during skeletal muscle regeneration

Marisella Panduro^{a,1}, Christophe Benoist^{a,b,2}, and Diane Mathis^{a,b,2}

^aDivision of Immunology, Department of Microbiology and Immunobiology, Harvard Medical School, Boston, MA 02115; and ^bEvergrande Center for Immunologic Diseases, Harvard Medical School and Brigham and Women's Hospital, Boston, MA 02115

Contributed by Diane Mathis, January 31, 2018 (sent for review January 12, 2018; reviewed by Jeffrey V. Ravetch and Emil R. Unanue)

Skeletal muscle regeneration is a highly orchestrated process that depends on multiple immune-system cell types, notably macrophages (MFs) and Foxp3⁺CD4⁺ regulatory T (T_{reg}) cells. This study addressed how T_{reg} cells rein in MFs during regeneration of murine muscle after acute injury with cardiotoxin. We first delineated and characterized two subsets of MFs according to their expression of major histocompatibility complex class II (MHCII) molecules, i.e., their ability to present antigens. Then, we assessed the impact of T_{reg} cells on these MF subsets by punctually depleting Foxp3⁺ cells during the regenerative process. T_{reg} cells controlled both the accumulation and phenotype of the two types of MFs. Their absence after injury promoted IFN- γ production, primarily by NK and effector T cells, which ultimately resulted in MF dysregulation and increased inflammation and fibrosis, pointing to compromised muscle repair. Thus, we uncovered an IFN- γ -centered regulatory layer by which T_{reg} cells keep MFs in check and dampen inflammation during regeneration of skeletal muscle.

macrophages | T_{reg} cells | muscle repair | interferon- γ | muscle regeneration

Skeletal muscle undergoes regeneration at steady state, in muscular dystrophies, and subsequent to acute injury, such as after cardiotoxin (CTX) treatment (1). Muscle damage initiates a highly orchestrated process, in which a pool of generally quiescent muscle progenitor cells, termed satellite cells, are activated (2, 3). Satellite cells undergo asymmetric division, proliferation, and differentiation into postmitotic precursors, which subsequently fuse into multinucleated myotubes. Myotubes then form new, or fuse to existing, myofibers and proceed through a stage of terminal differentiation and growth. While myogenic precursor cells are essential for muscle regeneration, they are not sufficient on their own. Several types of immunocytes also play key roles (4).

Macrophages (MFs) are important players in skeletal muscle repair. Ablation of the myeloid compartment, in particular MFs, by multiple approaches results in defective repair, prolonged necrosis, and increased adipogenesis and fibrosis in the injured muscle (5–7). MFs can sense injury, phagocytose debris, mount an inflammatory response, and promote muscle regeneration via secretion of insulin-like growth factor 1 (IGF1), growth differentiation factor 3 (GDF3) and, likely, other factors (8, 9). The function of muscle MFs changes with their phenotype over the course of regeneration. Proinflammatory MFs accumulate early upon injury and express abundant tumor necrosis factor (TNF)- α (6), which induces expression of myogenic transcription factors (10) and promotes apoptosis of profibrotic fibro/adipogenic progenitors (FAPs) (11). Switching of muscle MFs to a proregenerative phenotype results in higher production of transforming growth factor (TGF)- β (6), which stimulates survival of FAPs, with concomitant deposition of cell matrix in the regenerating muscle (11). While the phenotypic switch is necessary for efficient muscle repair (12–14), the mechanisms governing it are largely unknown.

T_{reg} cells accumulate in murine skeletal muscle after acute injury, within the dystrophic muscles of *mdx* mutant mice, and in the

muscle of patients with dystrophinopathies (15–17). Punctual depletion of muscle T_{reg} cells results in impaired regeneration, prolonged inflammation, and fibrosis (15, 16). Inefficient accumulation of T_{reg} cells upon injury also correlates with sarcopenia in aged mice, which can be improved by boosting muscle T_{reg} cells via injection of the cytokine, interleukin (IL)-33 (18). Loss of T_{reg} cells reduces the effectiveness of muscle progenitor cells, likely reflecting an impact of the growth factor, amphiregulin (15, 17). T_{reg} cells also regulate the inflammatory milieu surrounding the regenerating myofibers, notably the phenotype of muscle MFs (15, 16).

Here, we address the impact of muscle T_{reg} cells on MF accumulation and phenotype during murine skeletal muscle repair after acute injury. Our findings highlight a critical role for T_{reg} cells in reigning in a local IFN- γ response and, thereby, dampening proinflammatory MFs.

Results

Delineation of Distinct Subsets of Skeletal Muscle MFs According to MHCII Molecule Expression. Muscle MFs have often been parsed on the basis of Ly6c and/or CX3CR1 expression; however, neither of these markers has shown a strong association with phenotype after acute injury nor relevant in vivo functionality (6, 19). On the basis of potential functional divergence and our preliminary findings (i.e., differential sensitivity to T_{reg} loss; see

Significance

Skeletal muscle relies on its regenerative capacity to recover after acute injury. Immune-system cells, notably macrophages and regulatory T cells, play critical roles during muscle regeneration. This study addressed the impact of regulatory T cells on macrophages during muscle repair. In a mouse model of acute injury, regulatory T cells controlled the composition and phenotype of muscle macrophages during muscle repair by limiting production of the inflammatory cytokine, interferon- γ , produced by natural killer and effector T cells. Thus, we uncovered an interferon- γ -centered regulatory loop that can be further explored as a gateway to improved muscle therapies.

Author contributions: M.P., C.B., and D.M. designed research; M.P. performed research; M.P., C.B., and D.M. analyzed data; and M.P., C.B., and D.M. wrote the paper.

Reviewers: J.V.R., Rockefeller University; and E.R.U., Washington University.

The authors declare no conflict of interest.

Published under the PNAS license.

Data deposition: The data reported in this paper have been deposited in the Gene Expression Omnibus (GEO) database, <https://www.ncbi.nlm.nih.gov/geo> (accession no. GSE110308). Raw data pertinent to interferon- γ response signature can be retrieved from the GEO repository (accession no. GSE110549).

¹Present address: Surface Oncology, Cambridge, MA 02139.

²To whom correspondence may be addressed. Email: cbdm@hms.harvard.edu or dm@hms.harvard.edu.

This article contains supporting information online at www.pnas.org/lookup/suppl/doi:10.1073/pnas.1800618115/-DCSupplemental.

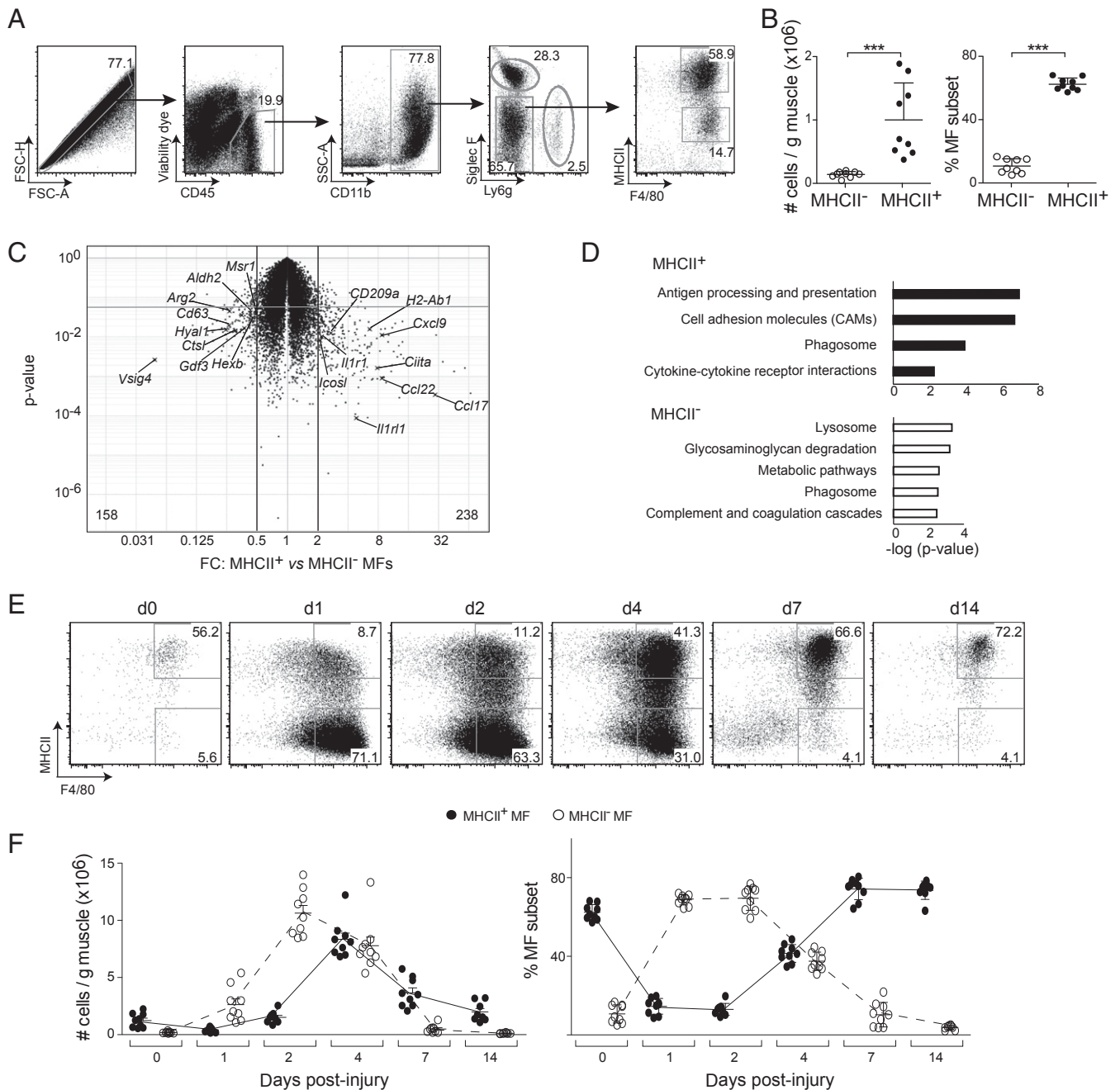


Fig. 1. Two subsets of MFs in skeletal muscle. (A) Gating strategy for cytofluorimetric delineation of skeletal muscle MF subsets at steady state. Numbers refer to fraction of cells within the designated gate. (B) Summaries of cell numbers (Left) and fractions (Right) of the MHCII⁺ and MHCII⁻ subsets from 6- to 10-wk-old male C57BL/6J mice. Three independent experiments. **P* < 0.05; ***P* < 0.01; ****P* < 0.001 by the unpaired *t* test. (C) Volcano plot of transcriptomic differences between the MHCII⁺ and MHCII⁻ MF subsets isolated from skeletal muscle at steady state. Averages of duplicate samples. (D) Pathway enrichment analysis (KEGG) of transcripts from ≥2-fold differentially expressed genes. *P* values represent maximum EASE score determined according to a modified Fisher Exact test (DAVID). Representative genes in these pathways are labeled in C. Cytofluorimetric dot plots (E) and quantification of cell number (F, Left) and frequency (Right) for MHCII⁺ vs. MHCII⁻ MF subsets during regeneration after acute injury with CTX. Results are from three individual experiments.

A Role for *T_{reg}* Cells in Regulating the Accumulation and Phenotype of Muscle MFs, we chose the gating strategy depicted in Fig. 1A, which culminates in a distinction based on MHCII expression by F4/80^{hi} cells. At steady state, the MHCII⁺ subset was more abundant than its MHCII⁻ counterpart (Fig. 1B). The MHCII⁻ subset showed more frequent and/or higher expression of CD64, Tim4, CX3CR1, CD206, and MerTK (Fig. S1A), all markers of tissue-resident MFs (20). However, the MHCII⁺ subset expressed more of the markers associated with migratory

MFs: CD11b, CCR2. Lack of substantial Ly6c expression by either subset (Fig. S1C) argues that our gating strategy identified bona fide MFs and excluded monocytes. MHCII⁻ MFs expressed higher levels of Ki67, a marker of cells in cycle (Fig. S1D), suggesting that this subset might have greater self-replenishing capacity, a property of tissue-resident MFs (21).

For a broader view, we compared the transcriptomes of MHCII⁺ and MHCII⁻ MFs via microarray (Fig. 1C and D). According to pathway enrichment analysis of genes differentially

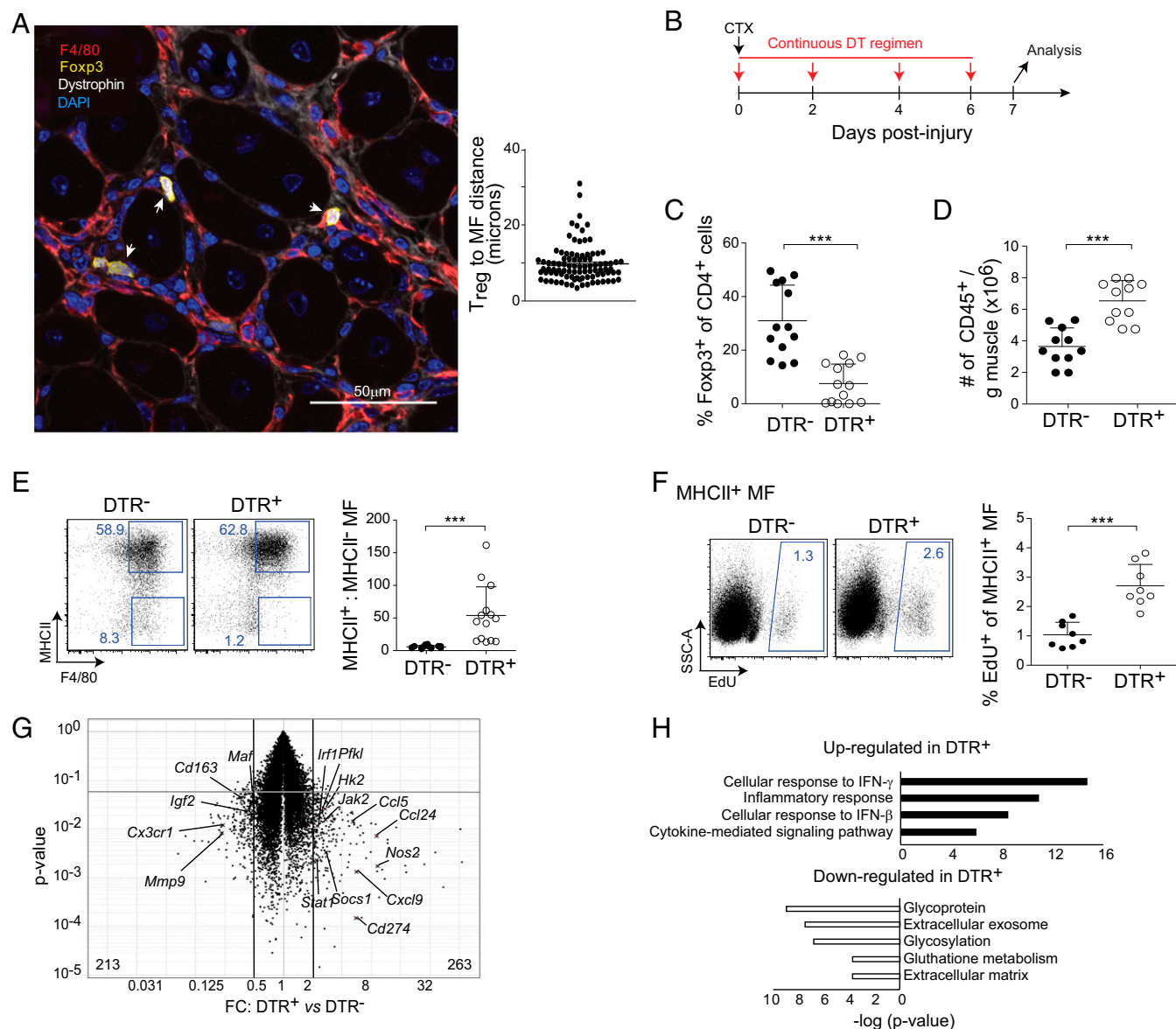


Fig. 2. Changes in MF representation and phenotype in the absence of T_{reg} cells. (A, Left) Immunofluorescence imaging of MFs and Foxp3⁺ T_{reg} cells in a cross-section of TA muscle at day 7 after injury with CTX. Original magnification 400× and 4× zoom. White arrows: T_{reg} cells and MFs within touching proximity. (A, Right) Quantification of the distances between T_{reg} cells and the nearest MF on day 7 after injury. Measured manually from 20 separate field views from three mice. (B) Continuous T_{reg} cell depletion regimen. (C–F) Analysis of diverse parameters following the regimen depicted in B: fraction of Foxp3⁺ T_{reg} cells (C); number of CD45⁺ cells per gram tissue (D); representative dot plots (E, Left) and quantification of MHCII⁺ to MHCII⁻ MF subset ratio (Right); representative dot plots and summary quantification of fraction of Edu⁺MHCII⁺ MF cells after a 4-h pulse just before tissue collection (F). DTR⁺, Foxp3^{DTR+} mice; DTR⁻, Foxp3^{DTR-} littermates. Numbers on dot plots refer to fraction of cells within the designated gates. Results are from three independent experiments. Statistics as per Fig. 1B. (G) Volcano plot comparing transcriptomes from MHCII⁺ MFs of T_{reg}-depleted (as per B) vs. nondepleted mice. (H) List of top pathways (KEGG) enriched in the sets of genes ≥twofold differentially expressed ($P < 0.05$). Representative genes in these pathways are indicated in G. Statistics are as per Fig. 1D. *** $P < 0.001$.

expressed ≥twofold, the MHCII⁺ subset up-regulated transcripts encoding molecules involved in antigen processing and presentation (*H2-Ab1*, *Ciita*), costimulation (*Icosl*), phagosomes (*CD209a*), and cytokine–cytokine receptor interactions (*Il6*, *Il1r1*, *Il1rl1*) (Fig. 1 C and D). However, the MHCII⁻ subset up-regulated transcripts associated with lysosomes (*CD63*, *Hexb*, *Ctsl*), glycosaminoglycan degradation (*Hyal*, *Hexb*), metabolic pathways (*Hyal1*, *Hexb*, *Arg2*, *Aldh2*), phagosomes (*Ctsl*, *Msr1*), and complement and coagulation cascades (*Vsig4*) (Fig. 1 C and D). While both MF types showed enrichment in transcripts involved in the phagosome pathway, different genes were involved in the two subsets. The MHCII⁻ subset also turned up transcripts

encoding the growth factor, GDF3 (Fig. 1C), a PPAR γ -dependent factor that potentiates muscle regeneration in vivo and promotes myofiber fusion in vitro (further discussed in Discussion) (9). There was little partitioning of the classical M1- and M2-type gene signatures (derived from Jablonski et al.; ref. 22) between the two subsets (Fig. S1E). There was more evident partitioning of certain gene signatures distilled by Xue et al. (23) for a set of polarization states of in vitro differentiated MFs: The MHCII⁻ subset showed greater expression of the signature in response to ultrapure LPS + immune complexes and to glucocorticoids (Fig. S1F).

Both the MHCII⁺ and MHCII⁻ MF subsets could be identified in normal skeletal muscle (Fig. S24). They often accumulated

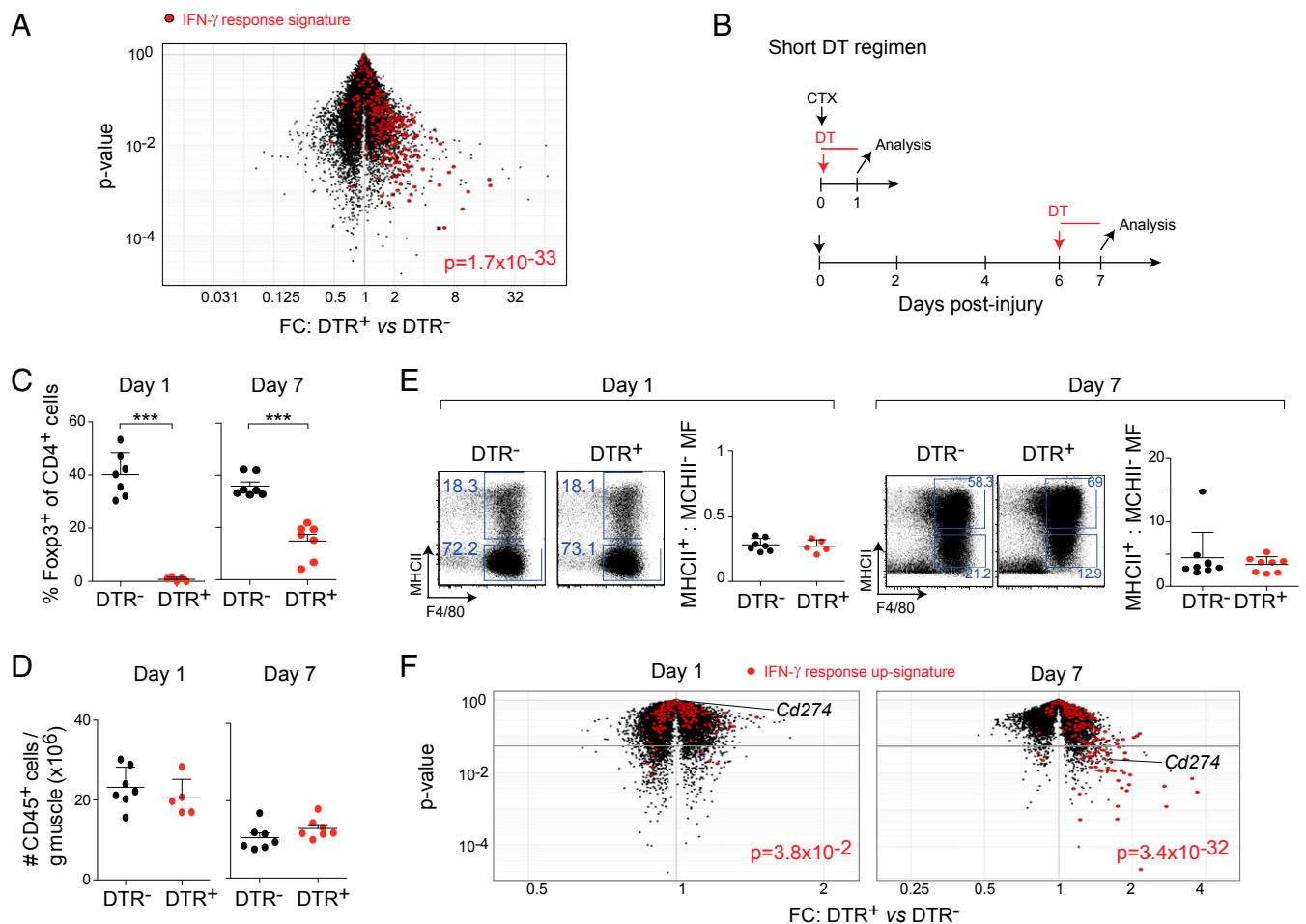


Fig. 3. An enhanced IFN- γ response in muscle MHCII⁺ MFs in the absence of T_{reg} cells. (A) Volcano plot as in Fig. 2H, except the IFN- γ response up-signature, detailed description in *Materials and Methods*, is highlighted in red. (B) DT injection regimens for short-term (24-h) depletion of T_{reg} cells at early or late phases of regeneration after injury with CTX, followed by analysis at the indicated time-points. Fraction of Fcpx3⁺CD4⁺ T_{reg} cells (C); number of CD45⁺ cells per gram of muscle (D); representative dot plots and summary quantification of MF subset ratios (E). Numbers on dot plots refer to fraction of cells within the designated gates. Data are from at least two independent experiments. Statistics are as in Fig. 1B. (F) Volcano plots of transcriptomes from MHCII⁺ MFs of DTR⁺ vs. DTR⁻ mice upon short-term depletion of T_{reg} cells beginning at day 1 or 7. Highlighted in red is the IFN- γ response up-signature, as in A. Averages of two to three replicates per group. *P* values according to the χ^2 test. ****P* < 0.001.

near autofluorescent myofibers, previously reported to be atrophic (24) (Fig. S2B).

We then asked how the two MF subsets evolved after acute injury of skeletal muscle with CTX. There was a rapid accumulation of MHCII⁻ MFs, peaking in number at day 2 and declining to preinjury levels by day 7, while MHCII⁺ MFs peaked in number at day 4 (Fig. 1E). Proportions of the two subsets reversed in dominance on days 1 and 2 but were restored to steady-state levels by day 7 (Fig. 1F). Transcriptome analyses revealed that the two MF subsets maintained their phenotypic distinction throughout the regeneration process, as signaled by enrichment of their respective steady-state signatures at all time-points (Fig. S3A).

Thus, we have delineated two phenotypically distinct subsets of MFs within steady-state skeletal muscle. While the MHCII⁻ subset seemed to be involved in homeostatic functions such as metabolism and degradation, the MHCII⁺ subset had the potential to be more engaged with other immunocytes via its capacity to present antigens and express chemokines. The latter MF type predominated in the later phases of acute muscle injury.

A Role for T_{reg} Cells in Regulating the Accumulation and Phenotype of Muscle MFs. MFs and T_{reg} cells colocalized in the regenerating areas of injured muscle, as illustrated for the tibialis anterior

(TA) on day 7 after CTX treatment (Fig. 2A). Most T_{reg} cells occurred within 10 μ m of a MF; in many cases, the two cell types were within touching distance.

To evaluate their impact on muscle MFs during the repair process, we punctually ablated T_{reg} cells in mice expressing the diphtheria toxin receptor (DTR) under the dictates of *Foxp3* regulatory elements [*Foxp3*-IRES-GFP-hDTR (Foxp3^{DTR})] (25). Every-other-day i.p. administration of diphtheria toxin (DT) during the week after CTX-induced injury (schematized in Fig. 2B) effectively reduced T_{reg} cells (Fig. 2C), resulting in a concomitant increase in CD45⁺ cells (Fig. 2D). The MHCII⁻ MF subset was strongly diminished during this same time period (Fig. 2E). An increased MHCII⁺ to MHCII⁻ MF ratio was not evident until day 7 (Fig. S4A). To assess how proliferation might contribute to this effect, we administered a 4-h pulse of 5-ethynyl-2'-deoxyuridine (EdU) on day 7 after injury to Foxp3^{DTR+} (T_{reg}-depleted) vs. Foxp3^{DTR-} (T_{reg}-replete) mice. MHCII⁺ MFs proliferated more actively in the absence of T_{reg} cells (Fig. 2F). There were too few MHCII⁻ MFs in the DTR⁺ mice to permit a parallel analysis of this subset.

Cytofluorimetric analysis of muscle MFs using canonical markers of tissue-resident MFs (20) revealed a decrease in expression of CD206, CX3CR1, and Tim4 in the MHCII⁺ subset in Foxp3^{DTR+} compared

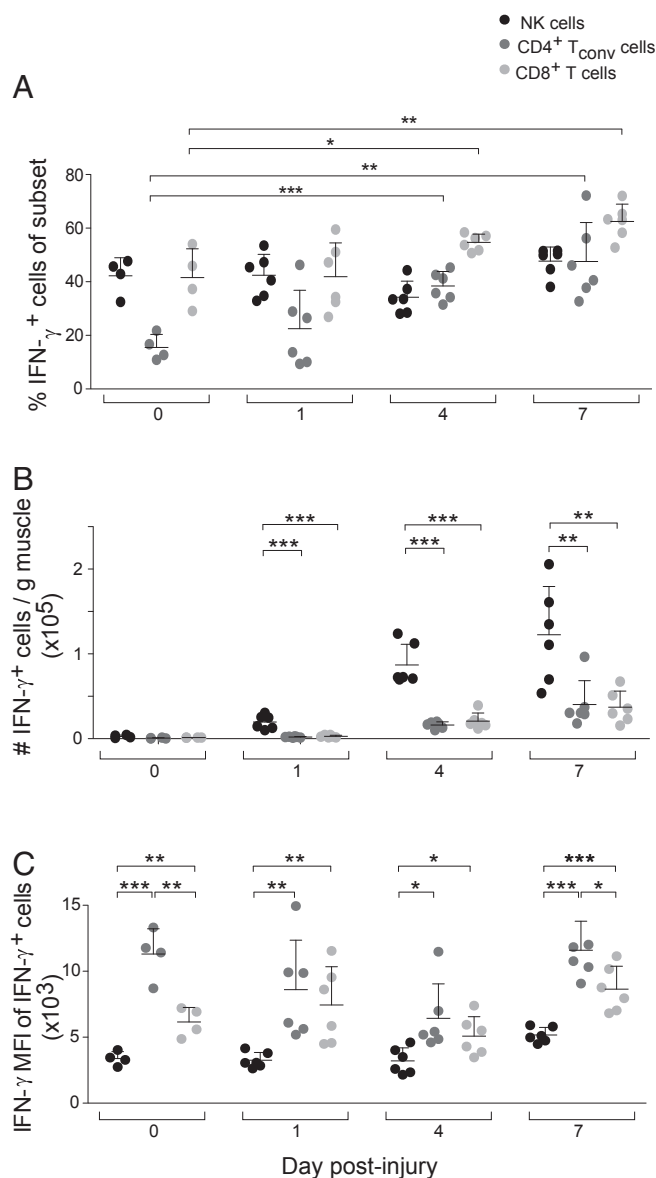


Fig. 4. Sources of muscle IFN- γ during muscle repair. (A–C) In T_{reg} -replete mice, quantification of the frequency (A), cell number per gram of muscle (B), and mean fluorescence intensity (MFI) (C) of IFN- γ synthesis by the designated cell types during regeneration after CTX-induced injury. Results are from two independent experiments. * $P < 0.05$; ** $P < 0.01$; *** $P < 0.001$.

with $Foxp3^{DTR-}$ mice; in contrast, inflammation-associated markers like CD11c and Ly6c were more highly expressed (Fig. S4 B and C). We expanded the analysis of MF phenotype by profiling transcriptomic changes in the MHCII⁺ subset from $Foxp3^{DTR+}$ vs. $Foxp3^{DTR-}$ mice on day 7 of regeneration (Fig. 2G). Transcripts up-regulated \geq twofold included a number associated with the response to IFN- γ (*Stat1*, *Socs1*, *Jak2*, *Irf1*, *Cd274*), the inflammatory response (*Nos2*, *Il1a*), cytokine-mediated signaling pathways (*Jak2*, *Stat1*, *Il1a*, *Socs1*), or chemotaxis (*Cxcl9*, *Ccl5*, *Ccl24*) (Fig. 2 G and H). We also observed down-regulation of genes potentially involved in homeostatic functions such as the glycoprotein pathway (*CD163*), extracellular exosome pathway, glycosylation, glutathione metabolism, and extracellular matrix (*Mmp9*), among others (Fig. 2H).

Therefore, T_{reg} cells were essential during muscle regeneration for the MF subsets to rebound to steady-state proportions. They

also stabilized the MF phenotype during the successive inflammatory and reparative phases of muscle regeneration.

During Muscle Regeneration, T_{reg} Cells Limited the Response of Local MFs to IFN- γ . We then turned to identifying the mechanisms by which T_{reg} cells regulated MF subset proportions and properties during muscle regeneration. Pathway analysis of transcripts overrepresented in MHCII⁺ MFs in the absence of T_{reg} cells pointed to an elevated response to IFN- γ (Fig. 2H). This notion was confirmed by overlaying an IFN- γ response up-signature onto a volcano plot of MHCII⁺ MF transcripts from DT-treated $Foxp3^{DTR+}$ vs. $Foxp3^{DTR-}$ mice (Fig. 3A). Analysis of the trajectory of the IFN- γ response signature revealed clusters of genes up-regulated in both MHCII⁺ and MHCII⁻ MFs at days 0, 1, 4, and 7 after injury (Fig. S5A). However, a large portion of the IFN- γ -induced signature genes was coregulated and highly overrepresented essentially only in MFs from $Foxp3^{DTR+}$ mice.

Next, we asked whether the IFN- γ response of MHCII⁺ MFs in T_{reg} -depleted mice reflected an accumulated effect throughout the 7 d of DT treatment, or whether shorter windows of T_{reg} insufficiency had a similar effect, as schematized in Fig. 3B. Short-term (24-h) DT treatment on either day 1 or 7 after injury depleted T_{reg} cells, although seemingly more effectively at the earlier time-point (Fig. 3C). However, neither the accumulation of CD45⁺ cells (Fig. 3D) nor the proportions of the two MF subsets (Fig. 3E) were significantly affected by these shorter T_{reg} -depletion regimens. Nonetheless, there was substantial up-regulation of the IFN- γ response up-signature by the MHCII⁺ MFs upon short-term T_{reg} cell depletion on day 7, i.e., the late phase of repair. Notably, *Cd274* transcripts, encoding PD-L1, a diagnostic IFN- γ -inducible gene, were clearly enriched. These data indicated that T_{reg} cells were required throughout the process of regeneration to limit an overexuberant MHCII⁺ MF response to IFN- γ produced in the context of regeneration.

Sources of Muscle IFN- γ and Their Regulation by T_{reg} Cells. To investigate which muscle lymphocytes produced IFN- γ during regeneration, we analyzed the dynamics of NK and effector T cell accumulation in the muscle and assessed their IFN- γ production potential upon ex vivo stimulation. About 40% of NK and CD8⁺ T cells were poised to produce IFN- γ at steady state, while half as many CD4⁺ T conventional (T_{conv}) cells exhibited this capacity (Fig. 4A). Upon injury, the fraction of IFN- γ ⁺ NK cells remained essentially constant, but that of the two effector T cell subsets increased subsequent to day 4 (Fig. 4A). NK cells were the most frequent IFN- γ producers (Fig. 4B), but their MFI was lowest (Fig. 4C).

To determine which IFN- γ -producing cells were under the control of T_{reg} cells, and to address when during regeneration T_{reg} cells were required to rein in IFN- γ production, we depleted them during either an early or late window of regeneration, compared with a continuous 1-wk depletion (regimens schematized in Fig. 5A). Despite a partial recovery of T_{reg} cells by day 7 (Fig. 5B), early ablation resulted in immunological effects similar to those of weeklong ablation: an increase in numbers of CD45⁺ cells (Fig. 5C), and an augmentation in IFN- γ -producing NK, CD4⁺ T_{conv} , and CD8⁺ T cells (Fig. 5D). In contrast, late ablation of T_{reg} cells had no significant impact on these parameters (Fig. 5 C and D) although the T_{reg} cell compartment rebounded less than after early depletion (Fig. 5B).

In brief, muscle T_{reg} cells were important in restraining NK and T cells and their potential to produce IFN- γ during regeneration. The T_{reg} cell effect on IFN- γ production required their presence early but not late after injury.

MHCII⁺ MFs Contributed to Type 1 Inflammation During Muscle Repair. Since T_{reg} cells controlled the proportion and phenotype of MFs during muscle regeneration, we asked whether antigen-presenting MFs played a role in the type 1 inflammation

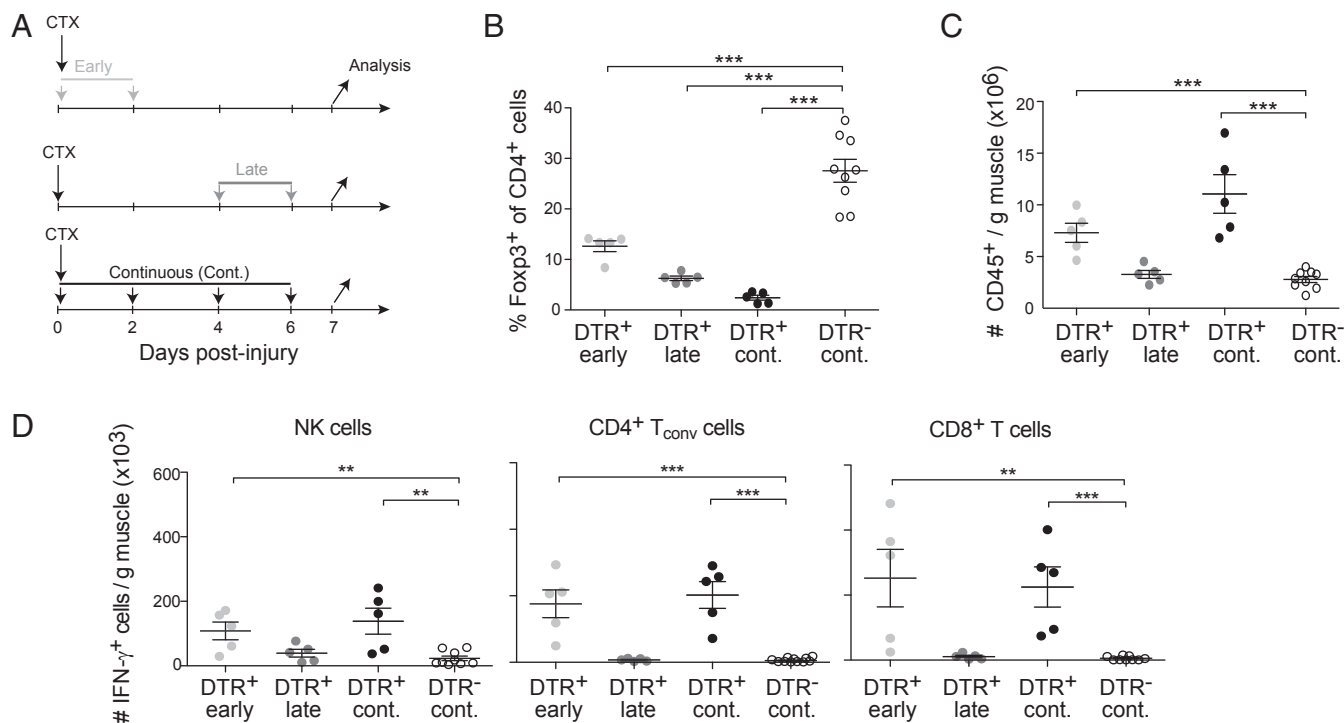


Fig. 5. Requirement for T_{reg} cells early after injury to limit $IFN-\gamma$ production. (A) DT-treatment regimens. Male DTR^+ or DTR^- littermates were 8–10 wk of age: fraction of $Foxp3^+CD4^+$ T_{reg} cells (B); number of $CD45^+$ cells (C); and quantification of $IFN-\gamma^+$ NK cells, $CD4^+$ T_{conv} , and $CD8^+$ T cells per gram of muscle (D). Data are from at least two independent experiments. Statistics are as per Fig. 1B. Cont., continuous. $**P < 0.01$; $***P < 0.001$.

induced by acute injury. To address this question, we used mice with *Ly2*-promoter/enhancer-driven ablation of *H2-Ab1* gene expression ($MF-MHCII^{-/-}$) (Fig. 6A). These mice and their wild-type littermates ($MF-MHCII^{+/+}$) showed comparable accumulation of $CD4^+$ $Foxp3^+$ T_{reg} and $Foxp3^-$ T_{conv} cells (Fig. 6B). However, there was a detectable decrease in the fraction of $IFN-\gamma^+CD4^+$ T_{conv} cells and in total numbers of $IFN-\gamma^+$ NK and $CD4^+$ T_{conv} cells in the mutant mice (Fig. 6C). Since $IFN-\gamma$ is known to induce MHCII expression in diverse cell types, these results suggest the existence of a positive feedback loop between accumulation of MHCII⁺ MFs and $IFN-\gamma^+$ leukocytes.

Effects of $IFN-\gamma$ on Repair of Skeletal Muscle. Increased production of and response to $IFN-\gamma$ in the absence of T_{reg} cells led us to directly investigate the role of $IFN-\gamma$ during muscle regeneration. We i.v.-injected recombinant (r) $IFN-\gamma$ into mice on days 4 and 6 after CTX-induced injury, and asked to what extent $IFN-\gamma$, alone, could mimic the effects of T_{reg} -cell ablation (Fig. 7A and B). Expression of PD-L1, an $IFN-\gamma$ -inducible gene, was augmented in muscle MFs of r $IFN-\gamma$ -treated mice (Fig. 7C). There was also an increase in the $CD45^+$ population (Fig. 7D) and elevated numbers of $IFN-\gamma^+$ NK and $CD4^+$ T_{conv} cells (Fig. 7E). Histological analysis of inflammation and fibrosis revealed that r $IFN-\gamma$ -treated (at 10 μ g per injection) mice had a significantly worse inflammation score (Fig. 7F) and a trend toward a higher fibrosis score (Fig. 7G) on day 7 of regeneration, which are indicators of ineffective muscle repair (26).

These data showed that injection of $IFN-\gamma$ alone could at least partially mimic the proinflammatory, antiregenerative effects of T_{reg} cell ablation. Moreover, $IFN-\gamma$ injection increased local production of $IFN-\gamma$.

Discussion

Acute injury of skeletal muscle provokes rapid accumulation of T_{reg} cells, which prevent excessive buildup of inflammatory myeloid cells and fibrosis in the regenerating muscle (15). This

study has refined our view of skeletal muscle MF subsets based on expression of F4/80 and MHCII. Most importantly, it established that T_{reg} cells keep inflammation in check by limiting $IFN-\gamma$ production in regenerating muscle. This finding raises a number of issues worthy of discussion.

First, skeletal muscle MFs have thus far been characterized as a bulk $CD11b^+$ population that expresses either the $Ly6c$ or $CX3CR1$ surface markers (6, 19). This delineation not only failed to identify bona fide MFs but did not uncover functionality associated with expression of either marker through muscle regeneration, for example (like us) no clear partitioning into M1 and M2 populations (19). By gating on $F4/80^{hi}$ MFs and parsing them according to MHCII expression, an indicator of antigen presentation, we identified two subsets of MFs that exhibited different transcriptional programs and, therefore, potential functions at steady state. Non-uniformity in expression of $CD64$, $Tim4$, $CX3CR1$, and $CD11c$ within the MHCII⁺ subset did suggest additional distinctions, but profiling at the single-cell level would be needed to fully resolve this heterogeneity. Cytofluorimetric and transcriptional analyses of the two MF subsets indicated that MHCII⁺ MFs were primarily proinflammatory, in particular, by promoting inflammation during muscle repair. In contrast, MHCII⁻ MFs showed enrichment in expression programs associated with tissue maintenance and proregenerative factors, such as $GDF3$. Thus, parsing MF subsets according to markers with a direct functional readout (i.e., antigen presentation) was an effective initial step toward understanding their heterogeneity and function.

Second, T_{reg} cells were found in close proximity to MFs and were required to preserve MF subset proportions and properties. The disproportion in MF subsets in the absence of T_{reg} cells could potentially reflect increased proliferation of the MHCII⁺ subset, greater conversion of the MHCII⁻ to MHCII⁺ cells, and/or death of the MHCII⁻ cells. Indeed, the MHCII⁺ subset had an elevated proliferation rate in the absence of T_{reg} cells. In addition, T_{reg} cells were essential for reining in NK and effector

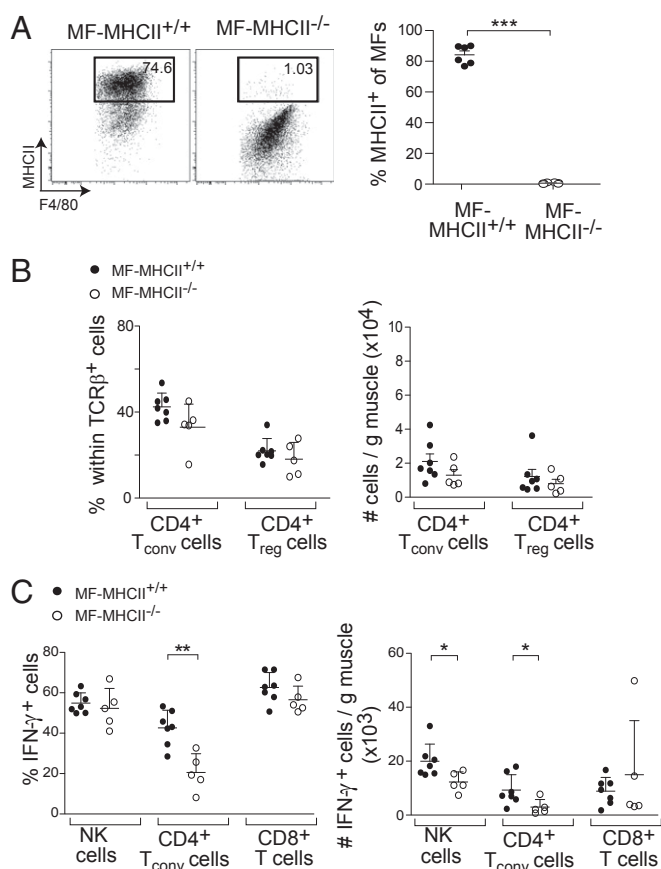


Fig. 6. Contribution of MHCII⁺ MFs to type 1 inflammation during muscle repair. (A) Representative dot-plot (Left) and summary data for fraction of MHCII⁺ MFs (Right) for MF-MHCII^{-/-} mice and wild-type littermate controls. Numbers refer to fraction of cells within the gate. (B) Fraction and number of CD4⁺ T_{conv} and T_{reg} cells in injured muscle of wild-type and mutant littermates. (C) Fraction and number of IFN-γ⁺ NK, CD4⁺ T_{conv}, and CD8⁺ T cells at day 14 after injury in WT and mutant littermates. Data are from two independent experiments. Statistics are as per Fig. 1B. **P* < 0.05; ***P* < 0.01; ****P* < 0.001.

T cells poised to produce IFN-γ, which is known to activate the transcription factor, CIITA, resulting in up-regulation of MHCII expression in MFs (27). Thus, by limiting local IFN-γ production, T_{reg} cells could prevent conversion of MHCII⁻ to MHCII⁺ MFs. Gain-of-function experiments showed that systemic injection of rIFN-γ partially recapitulated the effects on MF subset accumulation and phenotype observed in T_{reg}-depleted mice.

Third, while the presence of NK cells in regenerating skeletal muscle has been noted by a few groups (17, 28), their functional importance remains a question. We discovered that muscle NK cells were poised to produce IFN-γ already at steady state and that their numbers significantly increased after injury. While it is not clear precisely how T_{reg} cells controlled NK cells in the muscle, their quick mobilization argues in support of a direct impact. The relative importance of T_{reg} control of NK vs. effector T cell production of IFN-γ in this context is also not clear, but T_{reg} control of tissue-NK cells has been noted in several contexts in recent years. For instance, NK and T_{reg} cell numbers showed a reverse correlation in various tumors, in a TGF-β-dependent manner (29, 30). In addition, T_{reg} cells inhibited NK cell activation and cytotoxic function by acting as a sink for IL-2 in the contexts of type 1 diabetes and an in vivo model of recognition of missing-self (31, 32).

Last, we found that muscle T_{reg} cell function had a critical time window of efficacy. Punctual T_{reg}-ablation protocols dem-

onstrated that accumulation of T_{reg} cells was required early (initial few days after injury) to keep late-stage inflammation in check, in particular excessive local IFN-γ production by NK and effector T cells. It has been reported that IFN-γ is required for muscle regeneration after acute injury: It accumulates in the late phase of muscle repair, and its blockade or genetic deficiency inhibits regeneration (28). Furthermore, supplementation of IFN-γ in a laceration model reduced fibrosis and improved muscle function (33). However, it has also been demonstrated that IFN-γ can be detrimental in models of chronic muscle injury, wherein inflammation and fibrosis persist (34). It directly inhibited expression of the *Myog* gene, which encodes a crucial muscle differentiation factor up-regulated in the late stages of muscle regeneration, thereby dampening myogenesis (35, 36). We hypothesize that IFN-γ, while required for effective regeneration, must be tightly controlled temporally and quantitatively to prevent overt inflammation and persistent damage.

Acute skeletal muscle injury is common in sports and other traumatic accidents. A role for the immune system in potentiation of muscle repair is by now quite apparent (7, 15, 16). Immunotherapies are increasingly espoused in a broad range of clinical contexts. The T_{reg}:NK cell loop orchestrated through IFN-γ might provide a path to muscle immunotherapy.

Materials and Methods

Mice. C57BL/6J mice were purchased from Jackson Laboratory. B6.129P2-*Lyz2*^{tm1(cre)foj/j} (*LysM*^{Cre}) and B6.129 × *1-H2-Ab1*^{tm1Koni/j} (*MHCII*^{Flox}) mice were purchased from Jackson Laboratory and bred in our colony to generate MF-MHCII^{+/+} and MF-MHCII^{-/-} littermates. *Foxp3-IRES-GFP* (*Foxp3*^{GFP}) mice were obtained from V. Kuchroo, Brigham and Women's Hospital, Boston. *Foxp3-IRES-GFP-hDTR* (*Foxp3*^{DTR}) mice were obtained from A. Rudensky, Memorial Sloan-Kettering Cancer Center, New York. Six- to 10-wk-old male and female mice were used for all experiments, unless otherwise indicated. All mice were housed in our specific pathogen-free facility at Harvard Medical School. All experiments were conducted under protocols approved by Harvard Medical School's Institutional Animal Care and Use Committee.

Foxp3^{DTR+} and *Foxp3*^{DTR-} littermates were i.p.-injected with DT (Sigma-Aldrich, D0564) in phosphate-buffered solution (PBS) at 25 ng/g or 50 ng/g of body weight for continuous or short-term T_{reg} cell-depletion regimens, respectively. Protocols of DT administration for the different experiments are schematized in the corresponding figures. Male littermates were used in these experiments unless otherwise indicated. For in vivo rIFN-γ administration, 5–10 μg of IFN-γ (Biolegend) were i.v.-injected into mice in sterile PBS, according to the protocols detailed in the corresponding figures.

For acute injury, mice were anesthetized with avertin (0.4 mg/g body weight) and injected with 0.03 mL per muscle of *Naja mossaibica* CTX (0.03 mg/mL; Sigma-Aldrich) in one or more hindlimb muscles (TA, gastrocnemius, quadriceps), as previously described (15).

Isolation and Analysis of Muscle Leukocytes. Hindlimb muscles were excised, minced, and digested at 37 °C for 30 min in a solution containing collagenase II (2 mg/mL; Thermo Fisher Scientific), DNase I (150 μg/mL; Sigma-Aldrich), and Dulbecco's modified Eagle media (DMEM) without phenol red (Thermo Fisher Scientific). Digested muscle was passed through a 70 μm filter and washed in DMEM without phenol red/2% FBS/2 mM EDTA. To separate the leukocyte fraction, we resuspended the digested muscle in 40% Percoll (Sigma-Aldrich), underlain with 80% Percoll, and spun for 25 min at 1,126 × *g* (without breaks). The interphase containing leukocytes was recovered, washed, and stained for analysis or sorting by flow cytometry.

Samples were stained with the following antibodies: anti-CD3 (145-2C11), CD4 (GK1.5), CD8b (53-5.8), CD11b (M1/70), CD11c (N418), CD45 (30-F11), CD206 (C068C2), CX3CR1 (SA011F11), F4/80 (BM8), H2-A/E (M5/114.15.2), IFN-γ (XMG1.2), Ly6c (HK1.4), Ly6g (1A8), NK1.1 (PK136), PD-L1 (10F.9G2), TCRβ (H57-597), and Tim4 (F31-5G3), all from Biolegend; *Foxp3* (FJK-16s) from eBioscience; Siglec F (E50-2440) and Ki67 (B56) from BD Pharmingen; and MerTK (Polyclonal goat IgG) from R&D. Fixable viability dye Yellow (Thermo Fisher Scientific) was used to exclude dead cells in all experiments. Cytofluorimetric data were acquired with a 4-laser LSR II or 4-laser Fortessa (BD Biosciences) and were analyzed using FlowJo software (Tree Star).

For in vivo proliferation experiments, 1 mg of EdU (Thermo Fisher Scientific) was administered i.p. 4 h before analysis. After the tissue was collected, EdU detection was done after fixation and permeabilization using the

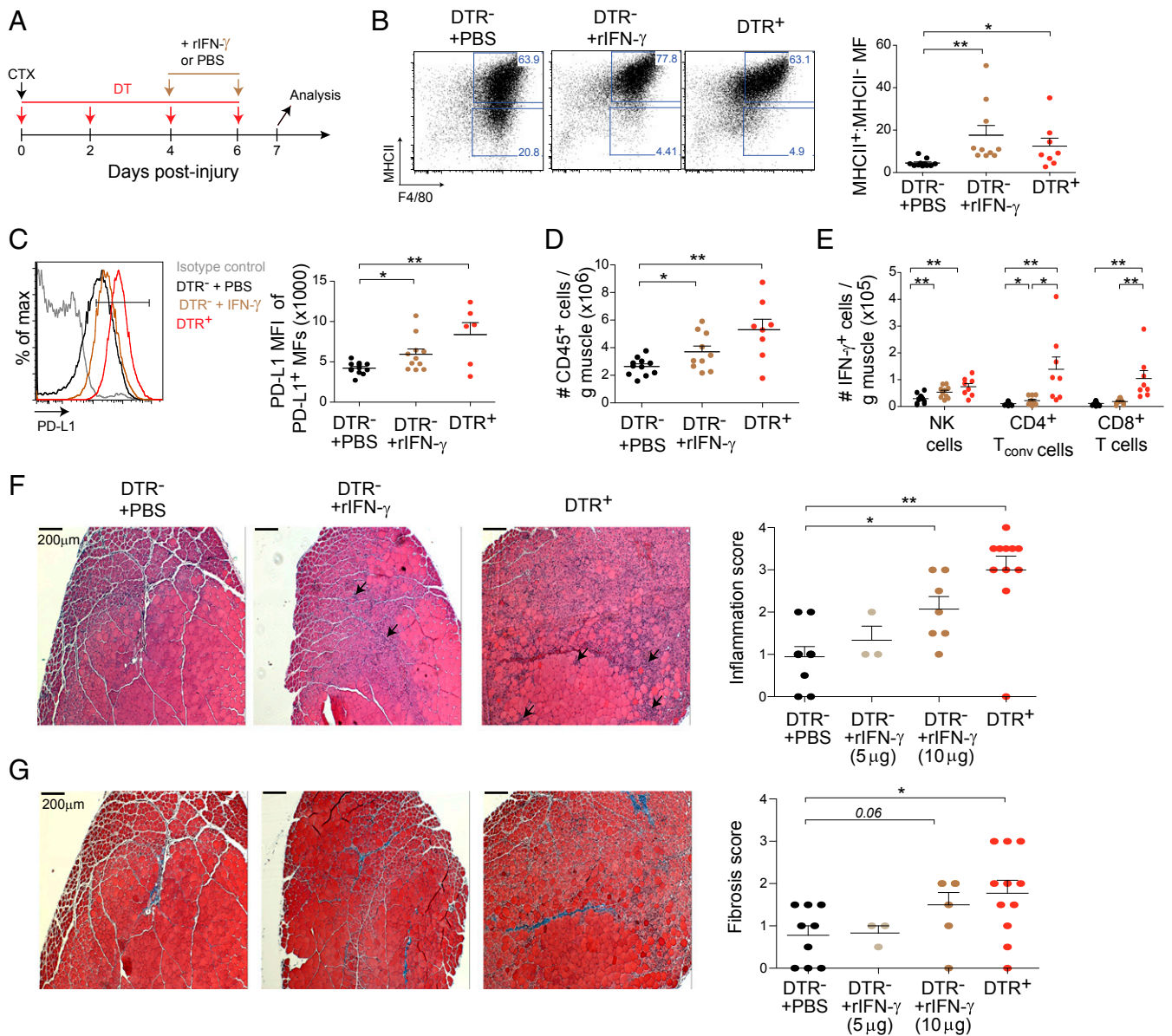


Fig. 7. Partial complementation of T_{reg} cell loss by $IFN-\gamma$ injection. (A) Strategy for evaluating the ability of $IFN-\gamma$ to compensate for T_{reg} cell loss (DTR^+) during muscle regeneration. $rIFN-\gamma$ was i.v.-injected into DTR^- mice twice as indicated. (B) Representative dot plots (Left) and summary quantification of MF subset ratios (Right). Numbers indicate fraction of cells in the designated gate. (C) Representative histogram (Left) and quantification (Right) of PD-L1 expression in PD-L1⁺ total muscle MFs. (D) Quantification of CD45⁺ cells per gram of muscle. (E) Quantification of $IFN-\gamma^+$ NK, CD4⁺ T_{conv} , and CD8⁺ T cells per gram of muscle. Results are from three independent experiments. (F) H&E histology: representative images (Left) and inflammation score (Right). Black arrows point to sites of inflammation. (Original magnification: 50 \times .) (Scale bars: 200 μ m.) Scoring was assessed by two-independent, blinded scorers. (G) Gomori Trichrome histology. As per F except fibrosis was assessed. All statistics as per Fig. 1B. * $P < 0.05$; ** $P < 0.01$.

Foxp3 Fix/Perm buffer set (eBioscience). The Click-iT EdU (Thermo Fisher Scientific) reaction was performed according to the manufacturer's instructions. Ki67 was stained intracellularly using the Foxp3 Fix/Perm buffer set.

For ex vivo intracellular $IFN-\gamma$ staining, muscle infiltrates were collected at the indicated time-points after injury, and single-cell suspensions were stimulated for 3.5 h at 37 $^{\circ}$ C with 50 ng/mL phorbol 12-myristate 13-acetate, 1 μ M ionomycin (both Sigma-Aldrich), and 1 \times GolgiPlug (BD Biosciences) in complete RPMI-1640 media, containing 10% FBS (Thermo Fisher Scientific), 1 \times penicillin/streptomycin (Gemini Bio Products), 10 mM sodium pyruvate (Thermo Fisher Scientific), 55 μ M β -mercaptoethanol (Sigma-Aldrich), 2 mM L-glutamine (Thermo Fisher Scientific). Cells were stained with fixable viability dye Yellow as above.

Transcriptome Analyses. Twenty thousand cells were double-sorted into TRIzol (Thermo Fisher Scientific). All samples were generated in duplicate or

triplicate. Sample processing and data analysis were performed as previously described (37). Extracted and amplified RNAs were hybridized to GeneChip Mouse Genome M1.0 ST chip arrays V2 (Affimetrix) according to the manufacturer's protocol. Microarray data are available from the National Center for Biotechnology Information (NCBI)/GEO repository under accession no. GSE110308. Data analysis was performed using GenePattern (Broad Institute) function Multiplot Studio. Heatmaps were generated using Gene-e (Broad Institute). Gene lists of interest were analyzed for pathway enrichment (KEGG) using DAVID Bioinformatics Resources 6.8 (38, 39).

$IFN-\gamma$ response up-regulated signature was derived from transcriptomes of peritoneal cavity MFs of C57BL/6J male mice injected s.c. with either 8,000 U of $rIFN-\gamma$ (Biologend), 10,000 U $IFN-\alpha$ (PBL Assay Science) or PBS (control) 2 h prior-analysis, as per protocol described in Mostafavi et al. (40). Cells were sorted and processed according to Immgen protocol for microarray analysis (41). Raw data can be retrieved from NCBI repository (superseries

GSE75306, subseries GSE110549 titled "Peritoneal cavity macrophage response to IFN γ and IFN α "). Criteria used to define said signature is as follows: CV < 0.08; mean > 100 in at least one sample; Fold-change (FC): IFN- γ /PBS \geq 2; $P \leq$ 0.05; FC: IFN- γ /IFN- α > 1. Signature was derived using averages from at least duplicate samples.

Immunofluorescence. TA muscles were fixed in 4% paraformaldehyde overnight, following a three-step dehydration process in 10%-20%-30% sucrose and snap-frozen in OCT in liquid nitrogen-chilled 2-methyl-butane. Frozen tissues were sectioned using a Microm HM550 cryostat (Thermo Fisher Scientific) and stored at -80°C . Slides were then soaked in PBS for 5 min and blocked for 1 h in 0.5% Triton X-100, 2% BSA, 0.5% donkey serum. Sections were stained with rat anti-F4/80 (Cl:A3-1, 1:50; Biolegend), rat anti-MHCII (M5/114.15.2, 1:50; Biolegend), mouse anti-dystrophin (MANDRA1, 1:300; Sigma). Rabbit polyclonal anti-GFP (1:200; Abcam) was used for detection of T_{reg} cells from Foxp3^{GFP} mice. Secondary stains were done using fluorescently conjugated donkey antibodies. Slides were mounted using Vectashield Mounting Media with DAPI (Vector Laboratories). Images were acquired using an Olympus Fluoview laser scanning microscope FV3000; objectives: UPLSAPO 20 \times , N.A.: 0.75 \times ; UPLFLN 40XO, N.A.: 1.3 \times ; Olympus FV315-SW Fluoview software; and were analyzed using ImageJ (Fiji). T_{reg} cell to nearest MF distance calculation was quantified manually by tracing a segment between nuclei of Foxp3⁺ and F4/80⁺ cells using ImageJ (Fiji) software.

Histology. Injured TA muscles were collected and fixed in 10% formalin. Tissues were processed at the Rodent Histopathology Core at Harvard Medical School for H&E (for inflammation) and Gomori's trichrome (for fibrosis) staining. Two sections, 200 μm apart, were recovered and stained for analysis. Images were acquired with a Zeiss Axio Imager.M1 microscope. Inflammation and fibrosis scorings were done blindly by two independent investigators. Averaged scores from the dual assessments were reported. Scoring scales: 0, none; 1, mild; 2, mild-moderate; 3, moderate; 4, severe.

Statistical Analyses. Data were routinely presented as mean \pm SD. * $P < 0.05$; ** $P < 0.01$, *** $P < 0.001$ from the unpaired t test using GraphPad Prism software. Volcano plot enrichment P values were determined via the χ^2 test using Microsoft Excel. Only significant P values are indicated on the various plots.

ACKNOWLEDGMENTS. We thank N. Asinovski, R. Cruse, K. Hattori, A. Ortiz-Lopez, H. Paik, A. Rhoads, K. K. Wang, L. Yang, G. Buruzula, and J. LaVecchio for experimental support; C. Laplace for graphics; and Drs. Mikael Pittet, Filip Swirski, Michael Carroll, Wilson Kuswanto, Dalia Burzyn, Julia Schanin, and James Mohan for helpful discussions. Cell sorting was performed at the Harvard Stem Cell Institute/Joslin Diabetes Center Flow Cytometry Core through NIH Grants P30DK036836 and S10OR021740, and this work was funded by NIH Grant R01 AR070334 and the JPB Foundation (to D.M.).

- Chargé SB, Rudnicki MA (2004) Cellular and molecular regulation of muscle regeneration. *Physiol Rev* 84:209–238.
- Sambasivan R, et al. (2011) Pax7-expressing satellite cells are indispensable for adult skeletal muscle regeneration. *Development* 138:3647–3656.
- Lepper C, Partridge TA, Fan CM (2011) An absolute requirement for Pax7-positive satellite cells in acute injury-induced skeletal muscle regeneration. *Development* 138:3639–3646.
- Tidball JG (2017) Regulation of muscle growth and regeneration by the immune system. *Nat Rev Immunol* 17:165–178.
- Summan M, et al. (2006) Macrophages and skeletal muscle regeneration: A clodronate-containing liposome depletion study. *Am J Physiol Regul Integr Comp Physiol* 290: R1488–R1495.
- Arnold L, et al. (2007) Inflammatory monocytes recruited after skeletal muscle injury switch into antiinflammatory macrophages to support myogenesis. *J Exp Med* 204: 1057–1069.
- Segawa M, et al. (2008) Suppression of macrophage functions impairs skeletal muscle regeneration with severe fibrosis. *Exp Cell Res* 314:3232–3244.
- Tonkin J, et al. (2015) Monocyte/macrophage-derived IGF-1 orchestrates murine skeletal muscle regeneration and modulates autocrine polarization. *Mol Ther* 23: 1189–1200.
- Varga T, et al. (2016) Macrophage PPAR γ , a lipid activated transcription factor controls the growth factor GDF3 and skeletal muscle regeneration. *Immunity* 45: 1038–1051.
- Chen SE, Jin B, Li YP (2007) TNF- α regulates myogenesis and muscle regeneration by activating p38 MAPK. *Am J Physiol Cell Physiol* 292:C1660–C1671.
- Lemos DR, et al. (2015) Nilotinib reduces muscle fibrosis in chronic muscle injury by promoting TNF-mediated apoptosis of fibro/adipogenic progenitors. *Nat Med* 21: 786–794.
- Ruffell D, et al. (2009) A CREB-C/EBP β cascade induces M2 macrophage-specific gene expression and promotes muscle injury repair. *Proc Natl Acad Sci USA* 106: 17475–17480.
- Deng B, Wehling-Henricks M, Villalta SA, Wang Y, Tidball JG (2012) IL-10 triggers changes in macrophage phenotype that promote muscle growth and regeneration. *J Immunol* 189:3669–3680.
- Mounier R, et al. (2013) AMPK α 1 regulates macrophage skewing at the time of resolution of inflammation during skeletal muscle regeneration. *Cell Metab* 18:251–264.
- Burzyn D, et al. (2013) A special population of regulatory T cells potentiates muscle repair. *Cell* 155:1282–1295.
- Villalta SA, et al. (2014) Regulatory T cells suppress muscle inflammation and injury in muscular dystrophy. *Sci Transl Med* 6:258ra142.
- Castiglioni A, et al. (2015) FOXP3⁺ T cells recruited to sites of sterile skeletal muscle injury regulate the fate of satellite cells and guide effective tissue regeneration. *PLoS One* 10:e0128094.
- Kuswanto W, et al. (2016) Poor repair of skeletal muscle in aging mice reflects a defect in local, IL-33-dependent, accumulation of regulatory T cells. *Immunity* 44: 355–367.
- Varga T, et al. (2016) Highly dynamic transcriptional signature of distinct macrophage subsets during sterile inflammation, resolution, and tissue repair. *J Immunol* 196: 4771–4782.
- Gautier EL, et al.; Immunological Genome Consortium (2012) Gene-expression profiles and transcriptional regulatory pathways that underlie the identity and diversity of mouse tissue macrophages. *Nat Immunol* 13:1118–1128.
- Jenkins SJ, et al. (2011) Local macrophage proliferation, rather than recruitment from the blood, is a signature of TH2 inflammation. *Science* 332:1284–1288.
- Jablonski KA, et al. (2015) Novel markers to delineate murine M1 and M2 macrophages. *PLoS One* 10:e0145342.
- Xue J, et al. (2014) Transcriptome-based network analysis reveals a spectrum model of human macrophage activation. *Immunity* 40:274–288.
- Cifuentes-Diaz C, et al. (2001) Deletion of murine SMN exon 7 directed to skeletal muscle leads to severe muscular dystrophy. *J Cell Biol* 152:1107–1114.
- Kim JM, Rasmussen JP, Rudensky AY (2007) Regulatory T cells prevent catastrophic autoimmunity throughout the lifespan of mice. *Nat Immunol* 8:191–197.
- Mann CJ, et al. (2011) Aberrant repair and fibrosis development in skeletal muscle. *Skelet Muscle* 1:21.
- Steege PS, Moore RN, Johnson HM, Oppenheim JJ (1982) Regulation of murine macrophage Ia antigen expression by a lymphokine with immune interferon activity. *J Exp Med* 156:1780–1793.
- Cheng M, Nguyen MH, Fantuzzi G, Koh TJ (2008) Endogenous interferon-gamma is required for efficient skeletal muscle regeneration. *Am J Physiol Cell Physiol* 294: C1183–C1191.
- Ghiringhelli F, et al. (2005) CD4+CD25+ regulatory T cells inhibit natural killer cell functions in a transforming growth factor-beta-dependent manner. *J Exp Med* 202: 1075–1085.
- Smyth MJ, et al. (2006) CD4+CD25+ T regulatory cells suppress NK cell-mediated immunotherapy of cancer. *J Immunol* 176:1582–1587.
- Sitrin J, Ring A, Garcia KC, Benoist C, Mathis D (2013) Regulatory T cells control NK cells in an insulinitis lesion by depriving them of IL-2. *J Exp Med* 210:1153–1165.
- Gasteiger G, et al. (2013) IL-2-dependent tuning of NK cell sensitivity for target cells is controlled by regulatory T cells. *J Exp Med* 210:1167–1178.
- Foster W, Li Y, Usas A, Somogyi G, Huard J (2003) Gamma interferon as an antifibrosis agent in skeletal muscle. *J Orthop Res* 21:798–804.
- Villalta SA, Deng B, Rinaldi C, Wehling-Henricks M, Tidball JG (2011) IFN- γ promotes muscle damage in the mdx mouse model of Duchenne muscular dystrophy by suppressing M2 macrophage activation and inhibiting muscle cell proliferation. *J Immunol* 187:5419–5428.
- Londhe P, Davie JK (2011) Gamma interferon modulates myogenesis through the major histocompatibility complex class II transactivator, CIITA. *Mol Cell Biol* 31: 2854–2866.
- Londhe P, Davie JK (2013) Interferon- γ resets muscle cell fate by stimulating the sequential recruitment of JARID2 and PRC2 to promoters to repress myogenesis. *Sci Signal* 6:ra107.
- Cipolletta D, et al. (2012) PPAR- γ is a major driver of the accumulation and phenotype of adipose tissue Treg cells. *Nature* 486:549–553.
- Huang da W, Sherman BT, Lempicki RA (2009) Systematic and integrative analysis of large gene lists using DAVID bioinformatics resources. *Nat Protoc* 4:44–57.
- Huang da W, Sherman BT, Lempicki RA (2009) Bioinformatics enrichment tools: Paths toward the comprehensive functional analysis of large gene lists. *Nucleic Acids Res* 37:1–13.
- Mostafavi S, et al.; Immunological Genome Project Consortium (2016) Parsing the interferon transcriptional network and its disease associations. *Cell* 164:564–578.
- Heng TS, Painter MW; Immunological Genome Project Consortium (2008) The immunological genome project: Networks of gene expression in immune cells. *Nat Immunol* 9:1091–1094.